Inorg. Chem. **2006**, *45*, 1656–1666

Multisite Effects on Intervalence Charge Transfer in a Clusterlike Trinuclear Assembly Containing Ruthenium and Osmium

Deanna M. D'Alessandro, Murray S. Davies, and F. Richard Keene*

School of Pharmacy and Molecular Sciences, James Cook University, Townsville, Queensland 4811, Australia

Received October 2, 2005

The intervalence charge transfer (IVCT) properties of the mixed-valence forms of the diastereoisomers of the dinuclear $[\{Ru(bpy)_2\}(\mu\text{-HAT})\{M(bpy)_2\}]^{5+}$ (M = Ru or Os) complexes and the trinuclear heterochiral $[\{Ru(bpy)_2\}_2\{Os(bpy)_2\}(\mu\text{-HAT})]^{n+}$ (n = 7, 8; HAT = 1,4,5,8,9,12-hexaazatriphenylene; bpy = 2,2′-bipyridine) species display a marked dependence on the nuclearity and extent of oxidation of the assemblies, while small differences are also observed for the diastereoisomers of the same complex in the dinuclear cases. The mixed-valence heterochiral $[\{Ru(bpy)_2\}_2\{Os(bpy)_2\}(\mu\text{-HAT})]^{n+}$ (n = 7, 8) forms exhibit IVCT properties that are intermediate between those of the diastereoisomeric forms of the localized hetero-dinuclear complex $[\{Ru(bpy)_2\}(\mu\text{-HAT})\{Os(bpy)_2\}]^{5+}$ and the borderline localized-to-delocalized homo-trinuclear complex $[\{Ru(bpy)_2\}_3(\mu\text{-HAT})]^{n+}$ (n = 7, 8). The near-infrared (NIR) spectrum of the +7 mixed-valence species exhibits both interconfigurational (IC) and IVCT transitions which are quantitatively similar to those in $[\{Ru(bpy)_2\}(\mu\text{-HAT})\{Os(bpy)_2\}]^{5+}$ and are indicative of the localized mixed-valence formulation $[\{Ru^{II}(bpy)_2\}_2\{Os^{III}(bpy)_2\}(\mu\text{-HAT})]^{7+}$. The +8 state exhibits a new band attributable to an IVCT transition in the near-infrared region.

Introduction

Intervalence charge transfer (IVCT) studies on mixed-valence complexes have provided crucial insights into the factors that govern electronic delocalization and the electron-transfer barrier, through the seminal theoretical formalism pioneered by Hush.[1,2] To date, IVCT studies have focused predominantly on dinuclear complexes of ruthenium and osmium, while experimental and theoretical studies on higher nuclearity polymetallic assemblies are relatively scarce, despite the potential of these studies to provide one of the most powerful and sensitive probes to elucidate aspects of intercomponent intramolecular electron transfer.[3−7] Of particular significance for dinuclear systems was the prediction of relationships between the parameters of the IVCT bands (specifically, the energy (ν_{max}), intensity (ϵ_{max}), and bandwidth ($\Delta\nu_{1/2}$)) and several factors which govern the activation barrier. According to the two-state classical theory,[1,2] the energy and bandwidth of the IVCT transition for a dinuclear system are given by

$$\nu_{max} = \lambda + \Delta E_0 + \Delta E' \quad (1)$$

$$\Delta\nu_{1/2}^{\circ} = [16RTln2(\lambda)]^{1/2} \quad (2)$$

The Franck−Condon factor (λ) corresponds to the sum of the reorganizational energies within the inner and outer sphere; the redox asymmetry (ΔE_0) is the thermodynamic energy difference between the two metal-based chromophores, and $\Delta E'$ reflects any additional energy contributions from spin−orbit coupling and ligand-field asymmetry.

The elucidation of multisite effects on electron-transfer phenomena in trinuclear complexes provides the link between the understanding of such processes in dinuclear species and in extended arrays and metallosupramolecular systems. A knowledge of the electron-transfer properties of the components, the bridging ligands, and their interdependence as a result of the molecular architecture of the assembly, results in the potential for control of useful processes. These include electron transfer along predetermined pathways, multielectron

* To whom correspondence should be addressed. Fax: +61-(0)7-4781-6078. Email: Richard.Keene@jcu.edu.au.

(1) Hush, N. S. *Progr. Inorg. Chem.* **1967**, *8*, 391−444.
(2) Hush, N. S. *Electrochim. Acta* **1968**, *13*, 1005−1023.
(3) Creutz, C. *Prog. Inorg. Chem.* **1983**, *30*, 1−73.
(4) Crutchley, R. J. *Adv. Inorg. Chem.* **1994**, *41*, 273−325.
(5) Kalyanasundaram, K.; Nazeeruddin, M. K. *Inorg. Chim. Acta* **1994**, *226*, 213−230.
(6) Ward, M. D. *Chem. Soc. Rev.* **1995**, *24*, 121−134.
(7) Demadis, K. D.; Hartshorn, C. M.; Meyer, T. J. *Chem. Rev.* **2001**, *101*, 2655−2685.

10.1021/ic051699i CCC: $33.50
Published on Web 01/27/2006

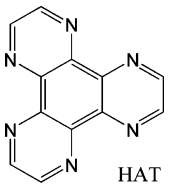

Figure 1.

exchange at a predetermined potential, and photoinduced charge separation.

IVCT studies in trinuclear complexes of ruthenium and osmium have focused predominantly on pyrazine-bridged chains,[8,9] complexes incorporating polypyridyl bridging ligands such as 2,3-dpp (2,3-bis(2-pyridyl)pyrazine)[10] and cyano-bridged tri- and tetranuclear complexes such as molecular squares and starburst structures.[11,12] However, there has been limited recognition of the stereochemical complexities inherent in such assemblies, and measurements on their physical properties have often been conducted on stereoisomeric mixtures.[13,14] Keene and co-workers reported the first examples of differences in the spectral, electrochemical, and photophysical properties of stereoisomers in mono-, di-, and trinuclear systems.[15−18] Stereochemical effects have also been shown to influence the IVCT properties of a range of dinuclear systems[19] including the diastereoisomers *meso*($\Delta\Lambda$)- and *rac*($\Delta\Delta/\Lambda\Lambda$)-[{Ru(bpy)$_2$}$_2$($\mu$-HAT)]$^{5+}$, and trinuclear systems, including homochiral (Δ_3/Λ_3)- and heterochiral ($\Delta_2\Lambda/\Lambda_2\Delta$)-[{Ru(bpy)$_2$}$_3$($\mu$-HAT)]$^{n+}$ (n = 7, 8), which are based on the bridging ligand HAT (bpy = 2,2′-bipyridine; HAT = 1,4,5,8,9,12-hexaazatriphenylene, shown in Figure 1).[20] The characteristics of the IVCT bands in the trinuclear case were markedly different from those of their dinuclear analogues because of the extensive electronic communication between the Ru(bpy)$_2^{2+}$ chromophores, and they varied significantly depending on the extent of oxidation and the overall geometry of the assembly.

The present study broadens this earlier investigation of the IVCT properties of homo-dinuclear and homo-trinuclear ruthenium systems[20] to the hetero-trinuclear system $\Delta_2\Lambda'/\Lambda_2\Delta'$-[{Ru(bpy)$_2$}$_2${Os(bpy)$_2$}($\mu$-HAT)]$^{6+}$ (where the prime denotes the stereochemistry of the Os center). The comparisons with the mononuclear complex [Os(bpy)$_2$(HAT)]$^{2+}$ and the diastereoisomers of the hetero-dinuclear [{Ru(bpy)$_2$}(μ-HAT){Os(bpy)$_2$}]$^{4+}$ and homo-dinuclear [{Os(bpy)$_2$}$_2$(μ-HAT)]$^{4+}$ systems provide a systematic basis for elucidating the influence of multisite interactions on the IVCT characteristics.

Experimental Section

Physical Measurements. 1D and 2D ^{1}H NMR spectra were performed using a Varian Mercury 300 MHz spectrometer. The ^{1}H NMR chemical shifts for all complexes are reported relative to 99.9% acetonitrile-d_3 (CD_3CN, Cambridge Isotope Laboratories (CIL)) at 1.93 ppm. ^{1}H NMR assignments were performed with the assistance of COSY experiments to identify each pyridine ring system.

Electrochemical measurements were performed under argon using a Bioanalytical Systems (BAS) 100A Electrochemical Analyzer. Cyclic (CV) and differential-pulse (DPV) voltammograms were recorded in a standard three-electrode cell using a glassy carbon or platinum button working electrode, a platinum wire auxiliary electrode, and an Ag/AgCl reference electrode (0.1 mol dm^{-3} [(n-C_4H_9)$_4$N]PF_6 in CH_3CN). Ferrocene was added as an internal standard upon completion of each experiment (the ferrocene/ferrocenium couple ([Fc]$^{+/0}$) occurred at +550 mV vs Ag/AgCl). Solutions contained 0.1 mol dm^{-3} [(n-C_4H_9)$_4$N]PF_6 as electrolyte. Cyclic voltammetry was performed with a sweep rate of 100 mVs^{-1}; differential pulse voltammetry was conducted with a sweep rate of 4 mVs^{-1} and a pulse amplitude, width, and period of 50 mV, 60 ms, and 1 s, respectively.

Elemental microanalyses were performed at the Microanalytical Unit in the Research School of Chemistry, Australian National University.

UV−vis/near-infrared (NIR) spectroelectrochemistry was performed using a CARY 5E spectrophotometer interfaced to Varian WinUV software. The absorption spectra of the electrogenerated mixed-valence species were obtained in situ by the use of a cryostatted optically semitransparent thin-layer electrosynthetic (OSTLE) cell, path length 0.605 mm, in an acetonitirle/0.1 M [(n-C_4H_9)$_4$N]PF_6 solution according to the methods detailed previously.[20] Since wavelength-dependent charge-transfer intensities scale with the inverse of the absolute absorption energy (ν^{-1}), plots of ϵ/ν versus ν are expected to exhibit a Gaussian shape rather than plots of ϵ versus ν (i.e., the "raw" experimental data).[1,21] The energy maximum of the "reduced" absorption spectrum (i.e., ϵ/ν vs ν) is identified with the vertical upper-/lower-surface energy separation and is the quantity most appropriately employed in the analysis of IVCT bands. The IVCT spectra were therefore scaled as $\int\epsilon(\nu)/\nu\, d\nu$,[1,21] and deconvolution of the NIR transitions was performed using the curve-fitting subroutine implemented within the GRAMS32 commercial software package, as described previously.[20] The Gaussian fits were not unique and the underlying components were obtained by first fitting a Gaussian peak at the maximum of the absorption band. A minimum number of additional Gaussians were subsequently included to obtain convergence in the iterative fitting procedure within GRAMS. On the basis of the reproducibility of the parameters obtained from the deconvolutions, the uncertainties in the energies (ν_{max}), intensities ($(\epsilon/\nu)_{max}$), and bandwidths ($\Delta\nu_{1/2}$) were estimated to be ±10 cm^{-1}, ±0.0001 M^{-1}, and ±10 cm^{-1}, respectively.

Materials. 2,2′-Bipyridine (bpy, Aldrich, 99+%), potassium hexafluorophosphate (KPF_6, Aldrich, 98%), hydrazine hydrate

(8) Powers, M. J.; Callahan, R. W.; Salmon, D. J.; Meyer, T. J. *Inorg. Chem.* **1976**, *15*, 894−900.
(9) von Kameke, A.; Tom, G. M.; Taube, H. *Inorg. Chem.* **1978**, *17*, 1790−1796.
(10) Serroni, S.; Campagna, S.; Denti, G.; Keyes, T. E.; Vos, J. G. *Inorg. Chem.* **1996**, *35*, 4513−4518.
(11) Oshio, H.; Onodera, H.; Tamada, O.; Mizutani, H.; Hikichi, T.; Ito, T. *Chem.−Eur. J.* **2000**, *6*, 2523−2530.
(12) Oshio, H.; Onodera, H.; Ito, T. *Chem.−Eur. J.* **2003**, *9*, 3946−3950.
(13) Keene, F. R. *Chem. Soc. Rev.* **1998**, *27*, 185−193.
(14) Keene, F. R. *Coord. Chem. Rev.* **1997**, *166*, 122−159.
(15) Kelso, L. S.; Reitsma, D. A.; Keene, F. R. *Inorg. Chem.* **1996**, *35*, 5144−5153.
(16) Rutherford, T. J.; Keene, F. R. *Inorg. Chem.* **1997**, *36*, 2872−2878.
(17) Rutherford, T. J.; Van Gijte, O.; Kirsch-De Mesmaeker, A.; Keene, F. R. *Inorg. Chem.* **1997**, *36*, 4465−4474.
(18) Treadway, J. A.; Chen, P.; Rutherford, T. J.; Keene, F. R.; Meyer, T. J. *J. Phys. Chem. A* **1997**, *101*, 6824−6826.
(19) D'Alessandro, D. M.; Kelso, L. S.; Keene, F. R. *Inorg. Chem.* **2001**, *40*, 6841−6844.
(20) D'Alessandro, D. M.; Keene, F. R. *Chem.−Eur. J.* **2005**, *11*, 3679−3688.
(21) Reimers, J. R.; Hush, N. S. *Inorg. Chem.* **1990**, *29*, 3686−3697.

(Aldrich), ethylene glycol (Ajax 95%), sodium toluene-4-sulfonate (Aldrich, 98%), DOWEX 1 × 8, 50−100 mesh (Aldrich) and Amberlite IRA-400 (Aldrich) anion-exchange resins (Cl^- form), 2,2,2-trifluoroethanol (TFE, Aldrich, 98%), and laboratory reagent solvents were used as received. Tetra-*n*-butylammonium hexafluorophosphate ($[n\text{-}C_4H_9)_4N]PF_6$, Fluka, 99+%) was dried in vacuo at 60 °C prior to use, and ferrocene (Fc, BDH) was purified by sublimation prior to use. SP Sephadex C-25, Sephadex LH-20 (Amersham Pharmacia Biotech), and silica gel (200−400 mesh, 60 Å, Aldrich) were employed for the chromatographic separation and purification of ruthenium complexes.[13] Silica gel (Fluka Kieselgel 60H, 5−40 μm) was used for liquid vacuum chromatography.[22] The ligand HAT was supplied by Dr. Nicholas Fletcher.

Immediately before use, acetonitrile (CH_3CN, Aldrich, 99.9+%) was distilled over CaH_2, and *N*,*N*-dimethylformamide (DMF, AR, Ajax) was stirred with 4 Å molecular sieves and distilled under reduced pressure (76 °C at 39 mmHg).

Complex Syntheses and Diastereoisomer Separation. *cis*-$[Ru(bpy)_2Cl_2]\cdot 2H_2O$ was prepared according to the literature procedure.[23] $[\{Ru(bpy)_2\}_2\{Os(bpy)_2\}(\mu\text{-HAT})](PF_6)_6$ was supplied by Dr Todd Rutherford,[24,25] and $(NH_4)_2[Os^{IV}Cl_6]$ was supplied by Dr Eric Jandrasics. The synthesis and characterization of $\Delta_2\Lambda'/\Lambda_2\Delta'$-$[\{Ru(bpy)_2\}_2\{Os(bpy)_2\}(\mu\text{-HAT})](PF_6)_6$, as well as the separation and purification of the respective diastereoisomers, was performed using the techniques reported previously.[17,24,25]

***cis*-$[Os(bpy)_2Cl_2]\cdot 2H_2O$.** *cis*-$[Os(bpy)_2Cl_2]\cdot 2H_2O$ was prepared via a modification of the literature procedure.[26,27] $(NH_4)_2[Os^{IV}Cl_6]$ (1.10 g, 2.51 mmol) was suspended in anhydrous DMF (20 cm^3) and refluxed at 160 °C with bpy (0.822 g, 5.26 mmol) for 1 h. During this time, crystals of NH_4Cl began to separate (after ca.15 min) and the initially dark red solution attained a brown coloration. After 1 h, the solution was filtered to remove NH_4Cl, and anhydrous methanol (15 cm^3) was added. *cis*-$[Os^{III}(bpy)_2Cl_2]Cl$ was subsequently precipitated from the filtrate as a light brown solid by the addition of diethyl ether (10 cm^3). The solid was isolated by vacuum filtration and washed with diethyl ether (3 × 10 cm^3). Yield: 1.50 g (98%). The ^1H NMR and UV−vis spectral characteristics were identical to those reported previously.[26,27]

cis-$[Os^{III}(bpy)_2Cl_2]Cl$ (1.00 g, 1.64 mmol) was dissolved in a minimum volume of warm methanol (ca. 100 cm^3), and hydrazine monohydrate (5 drops) was added dropwise with stirring to yield a dark purple/black solution. The addition of diethyl ether (100 cm^3) and the cooling of the solution in an ice-bath yielded a deep red/purple microcrystalline product of *cis*-$[Os^{II}(bpy)_2Cl_2]\cdot 2H_2O$ which was isolated by vacuum filtration and washed with diethyl ether (3 × 10 cm^3). Yield: 0.661 g (75%). The ^1H NMR and UV−vis spectral characteristics were identical to those reported previously.[26,27]

***rac*-$[Os(bpy)_2(HAT)](PF_6)_2$ and $[\{Os(bpy)_2\}_2(\mu\text{-HAT})](PF_6)_4$.** The synthesis and purification were performed via a procedure analogous to that reported previously for $[\{Ru(bpy)_2\}_2(\mu\text{-HAT})](PF_6)_4$[17] using *cis*-$[Os(bpy)_2Cl_2]\cdot 2H_2O$ as the precursor instead of *cis*-$[Ru(bpy)_2Cl_2]\cdot 2H_2O$.

A suspension of HAT (14.6 mg, 0.0623 mmol) in ethylene glycol (3 cm^3) was heated in a modified microwave oven (Sharp Model R-2V55, 600 W, 2450 MHz) on medium high power for 3 min to complete dissolution. *cis*-$[Os(bpy)_2Cl_2]\cdot 2H_2O$ (71.5 mg, 0.117 mmol) was added in four portions over 10 min during which time the solution attained a purple color. The crude mixture was diluted with distilled water (50 cm^3) and loaded onto a column of SP Sephadex C-25 (dimensions 25 × 3 cm). Separation of the desired dinuclear product from the mixture was achieved via the gradient elution procedure described by Masschelein et al.[28] A dark orange band of the mononuclear complex eluted first (0.20 M NaCl) followed by a dark purple band of the dinuclear complex (0.40 M NaCl). The complexes from the two bands were precipitated as their respective PF_6^- salts by the addition of a saturated solution of KPF_6. A blue band of the trinuclear species $[\{Os(bpy)_3\}_3(\mu\text{-HAT})]^{6+}$ was eluted with 0.6 M NaCl. The mono- and dinuclear complexes were isolated by vacuum filtration and washed with diethyl ether (3 × 10 cm^3). Yields: mononuclear complex, 27.0 mg; dinuclear complex, 67.7 mg (60%). ***rac*-$[Os(bpy)_2(HAT)](PF_6)_2$.** ^1H NMR (CD_3CN): δ 7.18 (H5′, 2H, J = 8, 5 Hz, dd), 7.48 (H5, 2H, J = 8, 5 Hz, dd), 7.50 (H6′, 2H, J = 5, 1.5 Hz, dd), 7.67 (H6, 2H, J = 5, 1.5 Hz, dd), 7.93 (H4′, 2H, J = 8, 8 Hz, dd), 8.00 (H4, 2H, J = 8, 8 Hz, dd), 8.34 (H2/H11 HAT, 2H, J = 3 Hz, d), 8.50 (H3′, 2H, J = 8, 1.5 Hz, dd), 8.57 (H3, 2H, J = 8, 1.5 Hz, dd), 8.82 (H3/H10 HAT, 2H, J = 3 Hz, d), 9,36 (H6/H7 HAT, 2H, s). **$[\{Os(bpy)_2\}_2(\mu\text{-HAT})](PF_6)_4$.** Anal. Calcd for $C_{52}H_{38}F_{24}N_{14}P_4Os_2$: C, 34.3; H, 2.11; N, 10.8. Found: C, 34.4; H, 2.50; N, 10.8. Further characterization was performed following diastereoisomer separation.

Separation of the diastereoisomers of $[\{Os(bpy)_2\}_2(\mu\text{-HAT})](PF_6)_4$ was achieved as detailed previously for $[\{Ru(bpy)_2\}_2(\mu\text{-HAT})]^{4+}$[24] using SP Sephadex C-25 support with 0.25 M sodium toluene-4-sulfonate solution as the eluent. Bands 1 and 2 were determined to be the meso and rac diastereoisomers, respectively, as established by ^1H and COSY NMR characterization and comparison with the ruthenium analogues. ^1H NMR (CD_3CN): δ (band 1, meso) 7.20 (H5d, 2H, J = 8, 5 Hz, dd), 7.36 (H5b, 2H, J = 8, 5 Hz, dd), 7.44 (H5c, 2H, J = 8, 5 Hz, dd), 7.50 (H5a, 2H, J = 8, 5 Hz, dd), 7.54 (H6d, 2H, J = 5, 1.5 Hz, dd), 7.62 (H6a, 2H, J = 5, 1.5 Hz, dd), 7.65 (H6c, 2H, J = 5, 1.5 Hz, dd), 7.76 (H6b, 2H, J = 5, 1.5 Hz, dd), 7.82 (H10/H11 HAT, 2H, s), 7.89 (H4d, 2H, J = 8, 8 Hz, dd), 7.93 (H4c, 2H, J = 8, 8 Hz, dd), 8.00 (H4b, 2H, J = 8, 8 Hz, dd), 8.02 (H4a, 2H, J = 8, 8 Hz, dd), 8.40 (H3d, 2H, J = 8, 1.5 Hz, dd), 8.44 (H2/H7 HAT, 2H, J = 3 Hz, d), 8.54 (H3c, 2H, J = 8, 1.5 Hz, dd), 8.52 (H3b, 2H, J = 8, 1.5 Hz, dd), 8.42 (H3a, 2H, J = 8, 1.5 Hz, dd), 8.87 (H3/H6 HAT, 2H, J = 3 Hz, d); (band 2, rac) 7.08 (H5b, 2H, J = 8, 5 Hz, dd), 7.32 (H5d, 2H, J = 8, 5 Hz, dd), 7.36 (H6b, 2H, J = 5, 1.5 Hz, dd), 7.41 (H5c, 2H, J = 8, 5 Hz, dd), 7.52 (H5a, 2H, J = 8, 5 Hz, dd), 7.52 (H6c, 2H, J = 5, 1.5 Hz, dd), 7.62 (H6d, 2H, J = 5, 1.5 Hz, dd), 7.65 (H6a, 2H, J = 5, 1.5 Hz, dd), 7.88 (H10/H11 HAT, 2H, s), 7.94 (H4b, 2H, J = 8, 8 Hz, dd), 7.95 (H4c, 2H, J = 8, 8 Hz, dd), 8.03 (H4b, 2H, J = 8, 8 Hz, dd), 8.06 (H4a, 2H, J = 8, 8 Hz, dd), 8.46 (H2/H7 HAT, 2H, J = 3 Hz, d), 8.51 (H3b, 2H, J = 8, 1.5 Hz, dd), 8.55 (H3c, 2H, J = 8, 1.5 Hz, dd), 8.55 (H3d, 2H, J = 8, 1.5 Hz, dd), 8.60 (H3a, 2H, J = 8, 1.5 Hz, dd), 8.89 (H6/H7 HAT, 2H, J = 3 Hz, d).

$[\{Ru(bpy)_2\}(\mu\text{-HAT})\{Os(bpy)_2\}](PF_6)_4$. $[\{Ru(bpy)_2\}(\mu\text{-HAT})\{Os(bpy)_2\}](PF_6)_4$ was synthesized in a manner similar to that described previously for the unsymmetric compound $[\{Ru(bpy)_2\}(\mu\text{-HAT})\{Ru(phen)_2\}](PF_6)_4$.[24,25]

$[Os(bpy)_2(HAT)](PF_6)_2$ (25.0 mg, 0.023 mmol) was added to a nitrogen-purged solution of methanol/water (1:1, 60 cm^3) and

(22) Coll, J. C.; Bowden, B. F. *J. Nat. Prod.* **1986**, *49*, 934−936.
(23) Togano, T.; Nagao, N.; Tsuchida, M.; Kumakura, H.; Hisamatsu, K.; Howell, F. S.; Mukaida, M. *Inorg. Chim. Acta* **1992**, *195*, 221−225.
(24) Rutherford, T. J.; Keene, F. R. *Inorg. Chem.* **1997**, *36*, 3580−3581.
(25) Rutherford, T. J.; Keene, F. R. *J. Chem. Soc., Dalton Trans.* **1998**, 1155−1162.
(26) Buckingham, D. A.; Dwyer, F. P.; Goodwin, H. A.; Sargeson, A. M. *Aust. J. Chem.* **1964**, *17*, 325−336.
(27) Jandrasics, E. Z.; Keene, F. R. *J. Chem. Soc., Dalton Trans.* **1997**, 153−159.
(28) Masschelein, A.; Kirsch-De Mesmaeker, A.; Verhoeven, C.; Nasielski-Hinkens, R. *Inorg. Chim. Acta* **1987**, *129*, L13−L16.

brought to reflux. $[Ru(bpy)_2Cl_2]\cdot 2H_2O$ (11.2 mg, 0.023 mmol) was dissolved in methanol/water, and the mixture added dropwise over several hours. The reaction mixture was refluxed for a further 12 h. The methanol was removed in vacuo, and the crude product was purified on SP Sephadex C-25 via the gradient elution procedure described above. A dark purple band of the dinuclear complex eluted with 0.40 M NaCl and was isolated as the PF_6^- salt by addition of a saturated solution of KPF_6. The solid was isolated by vacuum filtration and washed with diethyl ether (3×10 cm^3). Yield: 35.0 mg (88%). Anal. Calcd for $C_{52}H_{38}F_{24}N_{14}P_4OsRu$: C, 36.1; H, 2.21; N, 11.3. Found: C, 36.2; H, 2.53; N, 11.1. Further characterization was performed following diastereoisomer separation.

Separation of the diastereoisomers was achieved as detailed previously for the related complexes $[\{Ru(bpy)_2\}_2(\mu\text{-HAT})]^{4+}$.[24] Bands 1 and 2 were determined to be the $\Delta\Lambda/\Lambda\Delta$ and $\Delta\Delta/\Lambda\Lambda$ diastereoisomers, respectively, as established by ^{1}H and COSY NMR characterization and comparison with the homo-dinuclear ruthenium and osmium analogues. ^{1}H NMR (CD_3CN): δ (band 1, $\Delta\Lambda/\Lambda\Delta$) 7.21 (1H, $J = 8$, 5 Hz, dd), 7.28 (1H, $J = 8$, 5 Hz, dd), 7.36 (1H, $J = 8$, 5 Hz, dd), 7.45 (1H, $J = 8$, 5 Hz, dd), 7.45−7.63 (10H, m), 7.66 (1H, $J = 5$, 1.5 Hz, dd), 7.72 (2H, $J = 5$, 1.5 Hz, dd), 7.75 (1H, $J = 5$, 1.5 Hz, dd), 7.90 (1H, s), 7.95 (1H, $J = 8$, 8 Hz, dd), 8.01 (1H, $J = 8$, 8 Hz, dd), 8.04 (2H, $J = 8$, 8 Hz, dd), 8.10 (1H, s), 8.13 (1H, $J = 8$, 8 Hz, dd), 8.18 (1H, $J = 8$, 8 Hz, dd), 8.23 (1H, $J = 3$ Hz, d), 8.43 (1H, $J = 3$ Hz, d), 8.45 (2H, $J = 8$, 1.5 Hz, dd), 8.47 (2H, $J = 8$, 1.5 Hz, dd), 8.54 (1H, $J = 8$, 1.5 Hz, dd), 8.55 (1H, $J = 8$, 1.5 Hz, dd), 8.59 (1H, $J = 8$, 1.5 Hz, dd), 8.62 (1H, $J = 8$, 1.5 Hz, dd), 8.91 (1H, $J = 3$ Hz, d), 9.22 (1H, $J = 3$ Hz, d); (band 2, $\Delta\Delta/\Lambda\Lambda$) 7.07 (1H, $J = 8$, 5 Hz, dd), 7.14 (1H, $J = 8$, 5 Hz, dd), 7.31 (1H, $J = 8$, 5 Hz, dd), 7.31 (1H, $J = 5$, 1.5 Hz, dd), 7.39 (1H, $J = 8$, 5 Hz, dd), 7.41 (2H, $J = 5$, 1.5 Hz, dd), 7.63−7.47 (6H, m), 7.64 (2H, $J = 5$, 1.5 Hz, dd), 7.75 (2H, $J = 5$, 1.5 Hz, dd), 7.94 (1H, $J = 8$, 8 Hz, dd), 7.96 (1H, $J = 8$, 8 Hz, dd), 8.05 (1H, $J = 8$, 8 Hz, dd), 8.06 (1H, $J = 8$, 8 Hz, dd), 8.05 (1H, $J = 8$, 8 Hz, dd), 8.10 (1H, s), 8.12 (1H, $J = 8$, 8 Hz, dd), 8.17 (2H, $J = 8$, 8 Hz, dd), 8.43 (1H, $J = 3$ Hz, d), 8.47 (1H, $J = 3$ Hz, d), 8.48−8.50 (3H, m), 8.51 (2H, $J = 8$, 1.5 Hz, dd), 8.57 (2H, $J = 8$, 1.5 Hz, dd), 8.61 (1H, $J = 8$, 1.5 Hz, dd), 8.90 (1H, $J = 3$ Hz, d), 9.21 (1H, $J = 3$ Hz, d).

X-ray Crystallography. Single crystals of $\Delta\Lambda/\Lambda\Delta$-$[\{Ru(bpy)_2\}(\mu\text{-HAT})\{Os(bpy)_2\}](PF_6)_3\cdot Cl$ were grown by slow evaporation of a 70:30 2,2,2-trifluoroethanol/H_2O solution of the complex under ambient conditions in the absence of light. Crystals suitable for X-ray study were coated with Paratone-N and mounted onto glass fibers. X-ray data were collected on a Bruker SMART CCD diffractometer using the SMART software package.[29] Data sets were corrected for absorption using the program SADABS.[30] The structure was solved using direct methods and refined on F^2 using SHELX97[31] within the WinGX interface.[32] All non-hydrogen atoms were located; however, the data at high θ were poor, and refinement with anisotropic thermal parameters resulted in nonpositive definite ellipsoids for some atoms. This necessitated the use of the "soft" restraint ISOR for both ruthenium atoms. The C atoms in the bipyridyl rings were constrained using a rigid-bond restraint. Hydrogen atoms were placed in calculated positions. The Ru and Os atoms could not be unambiguously identified on the basis of electron densities, and so they were modeled as if each metal atom occupied 50% at each site. A summary of the data collection and refinement details is provided in Table S1 in the Supporting Information, and the atomic coordinates, hydrogen atom coordinates, anisotropic thermal parameters, bond lengths, and bond angles are provided in Tables S2−S6.

(29) *SMART−Area detector Software Package*; Siemens: Madison, WI, 1993.
(30) *SADABS−Area Detector Absorption Correction*; Siemens: Madison, WI, 1996.
(31) Sheldrick, G. M. *SHELX97−Programs for Crystal Structure Analysis*; Institute for Anorganische Chemie der Universität Göttingen: Göttingen, Germany, 1997.
(32) Farrugia, L. J. *J. Appl. Crystallogr.* **1999**, *32*, 837−838.

Results and Discussion

Synthesis, Separation and Structural Characterization. The syntheses of the mononuclear $[Os(bpy)_2(HAT)]^{2+}$ and dinuclear $[\{Os(bpy)_2\}_2(\mu\text{-HAT})]^{4+}$ complexes were performed using the microwave methodology reported for the synthesis of the analogous ruthenium species.[17] The heterodinuclear complex $[\{Ru(bpy)_2\}(\mu\text{-HAT})\{Os(bpy)_2\}]^{4+}$ was prepared by the thermal reaction of the precursor complexes $[Os(bpy)_2(HAT)]^{2+}$ with $[Ru(bpy)_2Cl_2]\cdot 2H_2O$ in methanol/water for 12 h, as the reaction using microwave conditions (as described above) met with limited success.

The separation of the diastereoisomeric forms of the dinuclear complexes $[\{Os(bpy)_2\}_2(\mu\text{-HAT})]^{4+}$ and $[\{Ru(bpy)_2\}(\mu\text{-HAT})\{Os(bpy)_2\}]^{4+}$ was achieved by cation exchange chromatography using SP Sephadex C-25 as the support with aqueous 0.25 M sodium toluene-4-sulfonate solution as eluent. In both cases, the band 1 and 2 eluates were determined to be, respectively, the meso and rac diastereoisomers for the former, and the "pseudo-meso" and rac forms for the latter, as established by NMR characterization. A crystal structure was obtained for the complex isolated from the band 1 eluate which confirms its assignment as the $\Delta\Lambda/\Lambda\Delta$ (pseudo-meso) diastereoisomer.

^{1}H NMR Characterization. One- and two-dimensional NMR techniques permitted structural characterization of the separated meso and rac diastereoisomers of $[\{Os(bpy)_2\}_2(\mu\text{-HAT})]^{4+}$ and the pseudo-meso and rac forms of $[\{Ru(bpy)_2\}(\mu\text{-HAT})\{Os(bpy)_2\}]^{4+}$. The assigment of the ^{1}H NMR spectra for the meso and rac diasteroisomers of the mono-, di-, and trinuclear assemblies based on HAT is well established.[24,25] Accordingly, the discussion of the ^{1}H NMR spectra here is restricted to the pertinent resonances which are distinctive for the two diastereoisomers. A complete listing of the ^{1}H NMR assigments was provided in the Experimental Section.

The atom-labeling scheme employed in the assigment of the ^{1}H NMR chemical shifts for the mononuclear, $[Os(bpy)_2(HAT)]^{2+}$, and dinuclear complexes, $[\{Os(bpy)_2\}_2(\mu\text{-HAT})]^{4+}$ and $[\{Ru(bpy)_2\}(\mu\text{-HAT})\{Os(bpy)_2\}]^{4+}$, is provided in Figure S1, Supporting Information. The coordinated bpy ligands exhibit the expected coupling constant values[33] ($J_{3,4} = 8$ Hz, $J_{3,5} = 1.5$ Hz, $J_{4,5} = 8$ Hz, $J_{4,6} = 1.5$ Hz, and $J_{5,6} = 5$ Hz} and coupling patterns based on the symmetry requirements of the complexes.

$[Os(bpy)_2(HAT)]^{2+}$. The C_2 point group symmetry of $[Os(bpy)_2(HAT)]^{2+}$ requires two nonequivalent py rings for each bpy ligand (which are themselves related by the 2-fold axis), in addition to three proton resonances for HAT. The

(33) Constable, E. C.; Lewis, J. *Inorg. Chim. Acta* **1983**, *70*, 251−253.

assignment of the chemical shifts was based on previous assignments for $[Ru(bpy)_2(HAT)]^{2+}$.[24] The H5′ and H5 bpy resonances are oriented over the planes of the adjacent bpy and HAT ligands, respectively, and are thus assigned to the most upfield resonances at 7.18 and 7.48 ppm ($J = 8$, 5 Hz, dd), respectively, because of the increased anisotropic interactions. The H6 and H7 HAT protons give rise to the most downfield singlet resonance at 9.36 ppm because of their orientation opposite to the shielding influence from the adjacent ligands.

$[\{Os(bpy)_2\}_2(\mu\text{-HAT})]^{4+}$. The meso and rac diastereoisomers possess C_s and C_2 point group symmetries, respectively, and may be distinguished on the basis of the differential anisotropic interactions experienced by the bpy protons (particularly H5/H5′ and H6/H6′) depending upon the stereochemical relationship of the two metal centers.

In the rac diastereoisomer, bpy ring b is oriented over the plane of the HAT ligand and the bpy ligand across the bridge such that the H5′ and H6′ protons of bpy ring b experience increased diamagnetic anisotropic effects. The H5′ proton of ring b was assigned as the most upfield resonance at 7.08 ppm ($J = 8$, 5 Hz, dd), while H6′ (ring b) was assigned to the 7.36 ppm ($J = 5$, 1.5 Hz, dd) resonance. By comparison, the H5′ and H6′ protons of bpy ring b are oriented approximately in the plane (and thus in the deshielding cone) of the equivalent bpy across the bridge in the meso diastereoisomer. The H5′ proton of ring d which is situated over the plane of the HAT ligand and approximately parallel to the magnetically equivalent bpy across the bridge experiences the largest anisotropic effect and is assigned as the most upfield resonance at 7.20 ppm ($J = 8$, 5 Hz, dd). ^{1}H COSY spectra permitted the assignment of the remaining resonances.

$[\{Ru(bpy)_2\}(\mu\text{-HAT})\{Os(bpy)_2\}]^{4+}$. The pseudo-meso ($\Delta\Lambda/\Lambda\Delta$) and rac ($\Delta\Delta/\Lambda\Lambda$) diastereoisomers both possess C_1 point group symmetry and exhibit ^{1}H NMR spectra with four nonequivalent bpy ligands (i.e., 40 magnetically nonequivalent proton resonances) in addition to 6 nonequivalent HAT resonances. The spectrum for each diastereoisomer of the hetero-dinuclear complex appeared as a convolution of the spectra of the homo-dinuclear Ru and Os analogues, with additional resonances due to the nonequivalence of the six HAT protons. Because of the coincidental equivalence of certain proton resonances, the assignment of the chemical shifts to specific protons was ambiguous in some cases; however, the chemical shifts of the bpy ligands in the two diastereoisomers of the hetero-dinuclear complex were approximately identical to those of the corresponding bpy ligands in the homo-dinuclear complexes with identical relative stereochemistries. In general, the proton resonances in the diastereoisomers of $[\{Os(bpy)_2\}_2(\mu\text{-HAT})]^{4+}$ occurred slightly upfield of the analogous positions in the diastereoisomers of $[\{Ru(bpy)_2\}_2(\mu\text{-HAT})]^{4+}$ because of the increased shielding influence of the Os center compared with Ru.[34] The assignment of the protons of the bpy ligands coordinated to the Os and Ru centers was possible for some

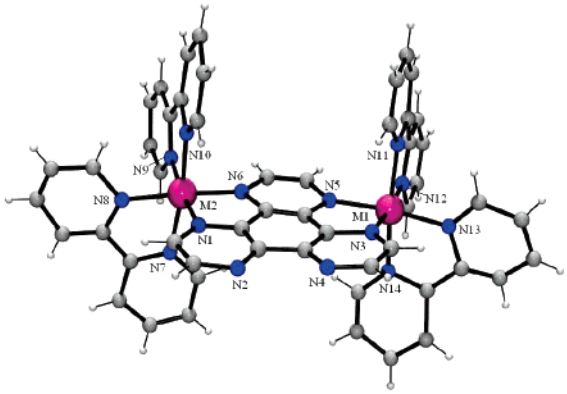

Figure 2. X-ray crystal structure of the cation in ΛΔ/ΔΛ-[{Ru(bpy)$_2$}-(μ-HAT){Os'(bpy)$_2$}](PF$_6$)$_3$·Cl with atom labeling.

resonances only, because of the highly convoluted nature of the spectra. The $\Delta\Delta/\Lambda\Lambda$ diastereoisomer exhibits the most upfield resonance at 7.07 ppm ($J = 8$, 5 Hz, dd) as the H5′ (ring b) proton of the bpy ligand coordinated to Os is oriented over the plane of the HAT ligand and the bpy ligand across the bridge. By comparison, the H5′ (ring d) bpy proton of the Os center is assigned to the most upfield resonance at 7.21 ppm ($J = 8$, 5 Hz, dd) in the $\Delta\Lambda/\Lambda\Delta$ diastereoisomer.

X-ray Crystallography. ΛΔ/ΔΛ-[{Ru(bpy)$_2$}(μ-HAT)-{Os(bpy)$_2$}](PF$_6$)$_3$·Cl crystallized in the monoclinic space group $P2_1/n$ with four dinuclear cations in the unit cell. A perspective view of the dinuclear cation is shown in Figure 2, and details of the bond lengths and angles are provided in Tables S5 and S6, Supporting Information. The average M−N distances and N−M−N angles at each center are consistent with those reported previously for polypyridyl complexes of Ru and Os.[35−41] An unambiguous assignment of the identity of M(1) and M(2) was not possible during the structural refinement procedure, and the refinement was performed by assigning 50% occupancy of Ru and Os to both sites. The inabilitity to assign the metal centers is probably a consequence of the racemic nature of the compound, where the two enantiomeric forms, ΛΔ and ΔΛ, crystallize in equal proportions.[42] With the assumption that the crystal is representative of the bulk solution, the first major band eluted from the column during diastereoisomer separation is confirmed as ΛΔ/ΔΛ (pseudo-meso).

(34) Kober, E. M.; Meyer, T. J. *Inorg. Chem.* **1983**, *22*, 1614−1616.

(35) Fletcher, N. C.; Junk, P. C.; Reitsma, D. A.; Keene, F. R. *J. Chem. Soc., Dalton Trans.* **1998**, 133−138.
(36) Bardwell, D.; Jeffery, J. C.; Joulie, L.; Ward, M. D. *J. Chem. Soc., Dalton Trans.* **1993**, 2255−2256.
(37) Bardwell, D. A.; Horsburgh, L.; Jeffery, J. C.; Joulié, L. F.; Ward, M. D.; Webster, I.; Yellowlees, L. J. *J. Chem. Soc., Dalton Trans.* **1996**, 2527−2531.
(38) Hage, R.; Haasnoot, J. G.; Nieuwenhuis, H. A.; Reedijk, J.; De Ridder, D. J. A.; Vos, J. G. *J. Am. Chem. Soc.* **1990**, *112*, 9245−9251.
(39) Balzani, V.; Bardwell, D. A.; Barigelletti, F.; Cleary, F. L.; Guardigli, M.; Jeffery, J. C.; Sovrani, T.; Ward, M. D. *J. Chem. Soc., Dalton Trans.* **1995**, 3601−3608.
(40) Baitalik, S.; Flörke, U.; Nag, K. *J. Chem. Soc., Dalton Trans.* **1999**, 719−727.
(41) Masui, H.; Freda, A. L.; Zerner, M. C.; Lever, A. B. P. *Inorg. Chem.* **2000**, *39*, 141−152.
(42) von Zelewsky, A. *Stereochemistry of Coordination Compounds*; Wiley: Chichester, U.K., 1995.

The bridging HAT ligand maintains planarity, and each metal center resides in a slightly disorted octahedral environment with an M(1)···M(2) separation of 6.834(10) Å. Two PF_6^- counterions were located within the clefts between the bipyridine rings at the pyrazine end of the bridging ligand rather than the end of the free nitrogen atoms of the HAT ligand, at approximately equivalent distances on either side of the plane of the bridging ligand, as shown in Figure S2, Supporting Information. The anions associate in closer proximity to the pyrazine end of the bridge which is farthest from the uncoordinated nitrogen atoms of HAT because of unfavorable electron repulsions with the PF_6^- anions which would occur in the latter case. The additional PF_6^- and Cl^- counterions reside outside the clefts and do not engage in any intermolecular interactions with the complex.

Electrochemistry and Electronic Spectroscopy. The electrochemical properties of $[Os(bpy)_2(HAT)]^{2+}$, the diastereoisomers of the dinuclear species $[\{Os(bpy)_2\}_2(\mu\text{-HAT})]^{4+}$ and $[\{Ru(bpy)_2\}(\mu\text{-HAT})\{Os(bpy)_2\}]^{4+}$, and the trinuclear complex $\Delta_2\Lambda'/\Lambda_2\Delta'$-$[\{Ru(bpy)_2\}_2\{Os(bpy)_2\}(\mu\text{-HAT})]^{6+}$ were investigated by cyclic and differential pulse voltammetry in acetonitrile containing 0.10 M $[(n\text{-}C_4H_9)_4N]PF_6$ and are provided in Table 1. The electrochemical properties of the diastereoisomeric forms of $[\{Ru(bpy)_2\}_2\{Os(bpy)_2\}(\mu\text{-HAT})]^{6+}$ have been reported previously.[24]

The mono-, di-, and trinuclear systems are characterized by one, two, and three reversible one-electron redox processes, respectively, corresponding to successive oxidation of the metal centers. The first oxidation in the heteronuclear systems is based at the osmium center because of the raised $d\pi$ level of Os versus Ru.[34] The first two metal-based redox processes in $\Delta_2\Lambda'/\Lambda_2\Delta'$-$[\{Ru(bpy)_2\}_2\{Os(bpy)_2\}(\mu\text{-HAT})]^{6+}$ occur at similar potentials to those in $[\{Ru(bpy)_2\}(\mu\text{-HAT})\{Os(bpy)_2\}]^{4+}$. The Ru-centered oxidation processes in $[\{Ru(bpy)_2\}(\mu\text{-HAT})\{Os(bpy)_2\}]^{4+}$ and $\Delta_2\Lambda'/\Lambda_2\Delta'$-$[\{Ru(bpy)_2\}_2\{Os(bpy)_2\}(\mu\text{-HAT})]^{6+}$ occur at potentials slightly cathodic of the corresponding processes in $[\{Ru(bpy)_2\}_2(\mu\text{-HAT})]^{4+}$ and $[\{Ru(bpy)_2\}_3(\mu\text{-HAT})]^{6+}$, respectively. A schematic illustration of the relative potentials of the metal-based oxidation processes for the series of mono-, di-, and trinuclear complexes is provided in Figure S3, Supporting Information.

All complexes exhibited multiple reversible ligand-based reductions in the cathodic region (Table S7, Supporting Information) which were assigned by analogy with the ruthenium species.[20,24,43] In all cases, the first reduction process is localized on the HAT ligand. The second reduction was also localized on the HAT ligand in the dinuclear complexes, and both the second and third reductions are HAT-based in the trinuclear complexes.[44] In the diastereoisomers of $[\{Os(bpy)_2\}_2(\mu\text{-HAT})]^{4+}$ and $[\{Ru(bpy)_2\}(\mu\text{-HAT})\{Os(bpy)_2\}]^{4+}$, the subsequent four reduction processes are assigned to sequential reductions of the terminal bpy ligands. The first one-electron bpy reduction occurs for a bpy coordinated to the osmium center in $[\{Ru(bpy)_2\}(\mu\text{-HAT})\{Os(bpy)_2\}]^{4+}$, followed by one-electron oxidation of a bpy coordinated to Ru. These assignments are supported by electrochemical studies for related di- and trinuclear osmium complexes incorporating polypyridyl bridging ligands such as 2,3-dpp.[45−49]

The ΔE_{ox} and the resultant K_c values for the complexes reported in Table 1 provide a semiquantitative assessment of the extent of electronic delocalization and stability of the mixed-valence species.[3,4,50] The K_c values for $[\{Os(bpy)_2\}_2(\mu\text{-HAT})]^{4+}$ suggest a two-orders of magnitude increase in the stability of the mixed-valence species compared with that of the analogous $[\{Ru(bpy)_2\}_2(\mu\text{-HAT})]^{4+}$ diastereoisomers because of the enhanced back-bonding ability of osmium relative to ruthenium.[49,50] Similar observations have been reported previously for related dinuclear osmium complexes incorporating polypyridyl bridging ligands such as 2,3-dpp and 2,5-dpp.[45−49] For the hetereo-dinuclear and hetero-trinuclear systems, ΔE_{ox} includes an additional energy contribution due to the redox asymmetry (ΔE_0) of the complex, which also leads to an increase in K_c.

The separations between the oxidation processes were sufficient to permit the electrochemical generation of the monooxidized +5 mixed-valence forms of the dinuclear complexes, in addition to the singly (+7) and doubly (+8) oxidized forms of the trinuclear complexes.

The complete UV−vis/NIR spectral data for the unoxidized, partially oxidized, and fully oxidized forms of the mono-, di-, and trinuclear systems (for the range 3050−30000 cm^{-1}) are provided in Table 1, and the spectra of $\Delta\Lambda/\Lambda\Delta$-$[\{Ru(bpy)_2\}(\mu\text{-HAT})\{Os(bpy)_2\}]^{n+}$, *meso*-$[\{Os(bpy)_2\}_2(\mu\text{-HAT})]^{n+}$, and $\Delta_2\Lambda'/\Lambda_2\Delta'$-$[\{Ru(bpy)_2\}_2\{Os(bpy)_2\}(\mu\text{-HAT})]^{n+}$ are shown in Figures 3 and 4, respectively. The spectrum of $[Os(bpy)_2(HAT)]^{n+}$ is provided in Figure S4 (Supporting Information) for comparison.

The spectra of the unoxidized (+4) homo- and hetero-dinuclear systems exhibit similar features over the 15 000−30 000 cm^{-1} region which are assigned as overlapping $d\pi(M^{II}) \rightarrow \pi^*(HAT)$ and $d\pi(M^{II}) \rightarrow \pi^*(bpy)$ singlet metal-to-ligand (^{1}MLCT) transitions (M = Ru, Os). The $\pi \rightarrow \pi^*$-(HAT) and $\pi \rightarrow \pi^*(bpy)$ transitions appear in the 30 000−50 000 cm^{-1} region. For the dinuclear osmium systems, additional bands appear in the 10 000−15 000 cm^{-1} region compared with the spectra of the corresponding $[\{Ru(bpy)_2\}_2(\mu\text{-HAT})]^{4+}$, which are assigned as a $d\pi(Os^{II}) \rightarrow \pi^*(HAT)$ transition to the lowest-triplet excited state (^{3}MLCT). Transitions of the same origin are also evident in the spectrum of $[Os^{II}(bpy)_2(HAT)]^{2+}$. The relative intensities of the ^{3}MLCT transitions are approximately doubled in the $[\{Os(bpy)_2\}_2(\mu\text{-HAT})]^{4+}$ diastereoisomers compared with those of $[\{Ru(bpy)_2\}(\mu\text{-HAT})\{Os(bpy)_2\}]^{4+}$, consistent with the number of Os centers present. For the hetero-dinuclear complex, the lowest-energy bands in the visible region consist of overlap-

(43) Rutherford, T. J. PhD Thesis, James Cook University, 1997.
(44) Jacquet, L.; Kirsch-De Mesmaeker, A. *J. Chem. Soc., Faraday Trans.* **1992**, *88*, 2471−2480.
(45) Richter, M. M.; Brewer, K. J. *Inorg. Chem.* **1992**, *31*, 1594−1598.
(46) Richter, M. M.; Brewer, K. J. *Inorg. Chem.* **1993**, *32*, 2827−2834.
(47) Denti, G.; Campagna, S.; Sabatino, L.; Serroni, S.; Ciano, M.; Balzani, V. *Inorg. Chem.* **1990**, *29*, 4750−4758.
(48) Richter, M. M.; Brewer, K. J. *Inorg. Chim. Acta* **1991**, *180*, 125−131.
(49) Goldsby, K. A.; Meyer, T. J. *Inorg. Chem.* **1984**, *23*, 3002−3010.
(50) Richardson, D. E.; Taube, H. *Coord. Chem. Rev.* **1984**, *60*, 107−129.

Table 1. UV−vis/NIR Spectral[a] Data of the Reduced Absorption Spectra for the Di- and Trinuclear Complexes at −35 and −15 °C, respectively, and Electrochemical[b] Data (in mV) and K_c Values[c] for the Di- and Trinuclear Complexes[d]

complex	$n+$	$\nu_{max} \pm 10$ (cm^{-1}) $(\epsilon/\nu)_{max} \pm 0.0001$ (M^{-1})	assignment	E_{ox1}	E_{ox2}	E_{ox3}	$\Delta E_{ox(2-1)}$ (K_c)[c]	$\Delta E_{ox(3-2)}$ (K_c)[c]
$[Os(bpy)_2(HAT)]^{n+}$	2	13 990 (0.1397)		736				
		sh 17 710 (0.2896)						
		20 200 (0.7398)						
		22 500 (0.7751)						
	3	**4400 (0.06467)**	$Os^{III} \rightarrow Os^{III}$					
		5110 (0.05579)	$Os^{III} \rightarrow Os^{III}$					
		10 410 (0.02731)						
		18 045 (0.2117)						
		20 227 (0.2647)						
		22 210 (0.2829)						
meso-$[\{Os(bpy)_2\}_2(\mu\text{-HAT})]^{n+}$	4	12 105 (0.8051)		712	1060		348	
		17 615 (1.1569)					(7.91×10^5)	
		22 600 (0.7927)						
	5	**4960 (0.08227)**	*e*					
		8195 (0.2980)	$Os^{II} \rightarrow Os^{III}$					
		11 100 (0.4065)						
		sh 15 670 (0.3826)						
		17 485 (0.7274)						
	6	**4325 (0.2757)**	$Os^{III} \rightarrow Os^{III}$					
		5080 (0.1629)	$Os^{III} \rightarrow Os^{III}$					
		6630 (0.0420)	$Os^{III} \rightarrow Os^{III}$					
		14 185 (0.3953)						
rac-$[\{Os(bpy)_2\}_2(\mu\text{-HAT})]^{n}+$	4	12 075 (0.7960)		720	1072		352	
		17 585 (1.1569)					(9.25×10^5)	
		22 490 (0.7780)						
	5	**4950 (0.07760)**	*e*					
		8200 (0.3152)	$Os^{II} \rightarrow Os^{III}$					
		11 105 (0.4197)						
		sh 15 775 (0.4078)						
		17 435 (0.7532)						
	6	**4270 (0.2855)**	$Os^{III} \rightarrow Os^{III}$					
		5030 (0.1409)	$Os^{III} \rightarrow Os^{III}$					
		6790 (0.02851)	$Os^{III} \rightarrow Os^{III}$					
		14 125 (0.4474)						
ΔΛ/ΛΔ-$[\{Ru(bpy)_2\}(\mu\text{-HAT})\{Os(bpy)_2\}]^{n+}$	4	12 730 (0.3302)		832	1408		576	
		17 660 (0.9994)					(5.79×10^9)	
		23 610 (0.6971)						
	5	**4090 (0.4837)**	$Os^{III} \rightarrow Os^{III}$					
		4863 (0.1172)	*e*					
		8640 (0.1757)	$Ru^{II} \rightarrow Os^{III}$					
		13 990 (0.1220)						
		17 690 (0.6203)						
		25 830 (0.3897)						
	6	**4430 (0.2669)**	$Os^{III} \rightarrow Os^{III}$					
		5170 (0.1102)	$Os^{III} \rightarrow Os^{III}$					
		10 760 (0.7979)						
		13 260 (0.5192)						
		17 810 (0.1614)						
ΔΔ/ΛΛ-$[\{Ru(bpy)_2\}(\mu\text{-HAT})\{Os(bpy)_2\}]^{n+}$	4	12 760 (0.3403)		834	1410		576	
		17 650 (0.9993)					(5.79×10^9)	
		23 580 (0.6765)						
	5	**4080 (0.4577)**	$Os^{III} \rightarrow Os^{III}$					
		4860 (0.1434)	*e*					
		8650 (0.1635)	$Ru^{II} \rightarrow Os^{III}$					
		14 020 (0.1480)						
		17 550 (0.6990)						
		25 620 (0.3641)						
	6	**4000 (0.2544)**	$Os^{III} \rightarrow Os^{III}$					
		4720 (0.1115)	$Os^{III} \rightarrow Os^{III}$					
		8490 (0.1303)						
		10 740 (0.2007)						
		13 520 (6359)						
		17 470 (0.2943)						
		20 690 (0.2165)						
$\Delta_2\Lambda'/\Lambda_2\Delta'$-$[\{Ru(bpy)_2\}_2\{Os(bpy)_2\}(\mu\text{-HAT})]^{n+}$	6	*sh* 12 235 (0.3644)		904	1440	1680	536	240
		16 935 (1.88623)					(1.22×10^9)	(1.17×10^4)
		*sh*19 285 (1.2245)						
		24 155 (0.6670)						
		25 875 (0.5779)						
	7	**3966 (0.5169)**	$Os^{III} \rightarrow Os^{III}$					
		7707 (0.2221)	$Ru^{II} \rightarrow Os^{III}$					
		18 055 (1.3438)						
		sh 25 845 (0.4681)						
	8	**4070 (0.4512)**	$Os^{III} \rightarrow Os^{III}$					
		10 585 (0.5417)	$Ru^{II} \rightarrow Os^{III}$					
		13 500 (0.6279)						
		16 203 (12173)						
		19 050 (0.8669)						
	9	13 625 (0.9870)						

[a] Spectroelectrochemical experiments were conducted at −35 °C for the mono- and dinuclear species and at −15 °C for the trinuclear species, respectively; *sh* = shoulder of band. [b] All potentials (+3 mV) in 0.1 M $[(n\text{-}C_4H_9)_4N]PF_6/CH_3CN$ at +25 °C vs Fc^+/Fc^0. [c] K_c values determined from $K_c = exp(\Delta E_{ox}F/RT)$ where $F/RT = 38.92\ V^{-1}$ at 298 K.[3] [d] The absorbances of IVCT or IC origin are indicated in bold type, and their corresponding assignments are shown. [e] Vibronic transitions.

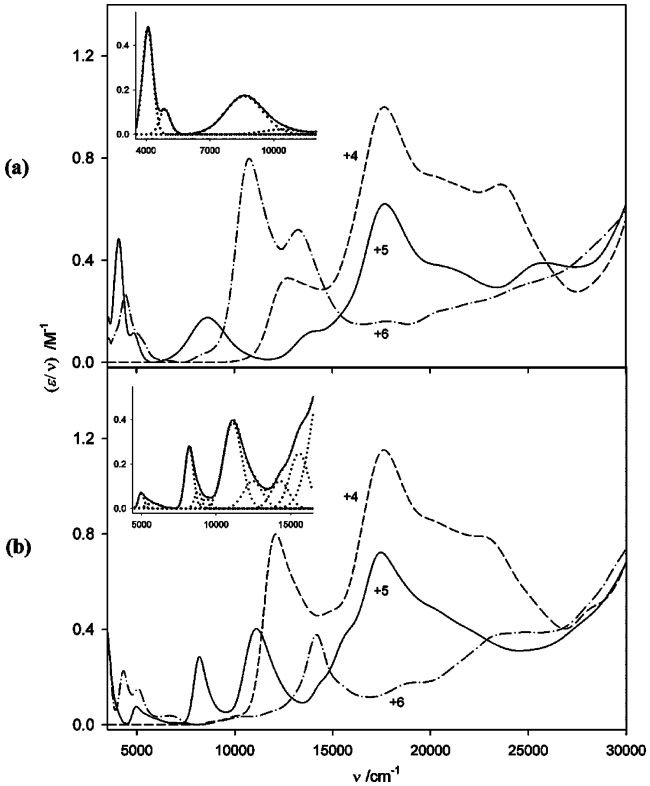

Figure 3. UV−vis/NIR spectra of the reduced absorption spectra of (a) ΔΛ/ΛΔ-[{Ru(bpy)$_2$}(μ-HAT){Os(bpy)$_2$}]$^{n+}$ and (b) *meso*-[{Os(bpy)$_2$}$_2$(μ-HAT)]$^{n+}$ (n = 4 (- - -), 5 (—), 6 (- · -)) at −35 °C. The insets show the bands obtained by Gaussian deconvolution of the NIR spectrum for the n = 5 (mixed-valence) species.

ping dπ(Os) → π*(HAT) and dπ(Ru) → π*(HAT) ^{3}MLCT and ^{1}MLCT transitions with the Os component occurring at lower energy in both cases.

The lowest-energy ^{3}MLCT and ^{1}MLCT transitions are progressively red shifted as the nuclearity of the assembly increases through the series [Os(bpy)$_2$(HAT)]$^{2+}$, [{Ru(bpy)$_2$}(μ-HAT){Os(bpy)$_2$}]$^{4+}$, and [{Ru(bpy)$_2$}$_2$Os(bpy)$_2$}(μ-HAT)]$^{6+}$, as the π* LUMO of the bridging ligand is progressively stabilized by interactions with the additional metal centers.[45−49] Minor differences were observed in the band energies and intensities between the diastereoisomers of the partially and fully oxidized di- and trinuclear systems.

Spectroelectrochemical generation of the dinuclear mixed-valence (+5) and fully oxidized (+6) forms of the dinuclear complexes revealed stable isosbestic points in the spectral progressions accompanying both oxidation processes. The ^{1}MLCT absorption bands decreased in intensity, experienced a slight red shift following one-electron oxidation, and eventually disappeared upon further oxidation to the +6 species. The ^{3}MLCT absorption bands also decreased in intensity, experienced a red shift in the homo-dinuclear osmium species, and disappeared completely following two-electron oxidation. The ^{3}MLCT absorption band disappeared completely following the one-electron oxidation in the hetereodinuclear complexes, consistent with the presence of a single Os center. LMCT transitions, π(bpy) → dπ(Os^{III}), in the +5 spectra of the dinuclear complexes appear at ∼14000 cm^{-1} as low-energy shoulders on the ^{1}MLCT transitions.

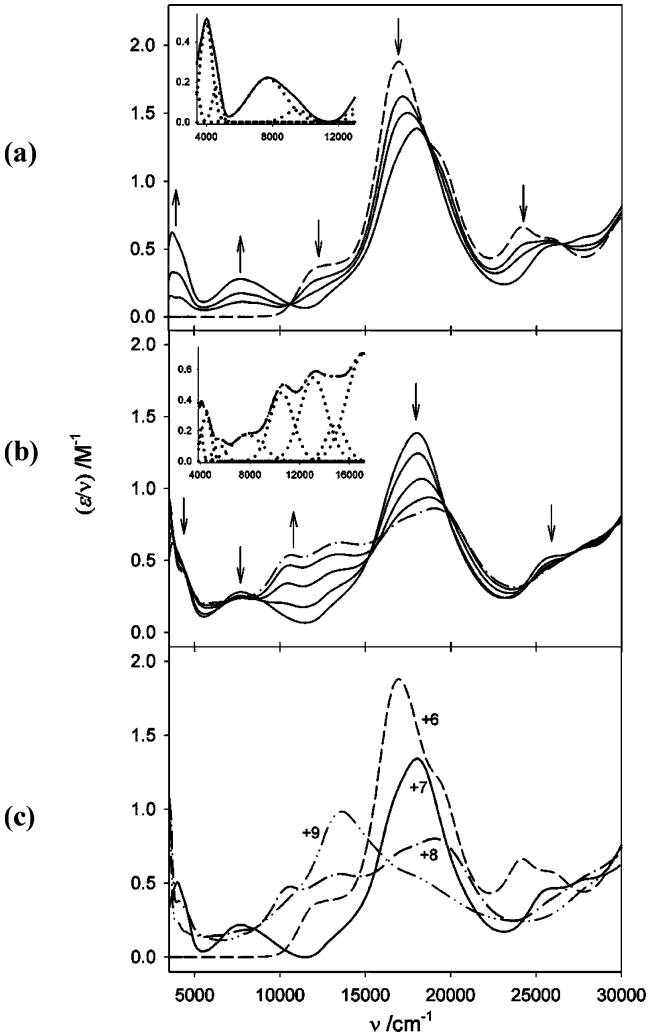

Figure 4. Spectroelectrochemistry for the oxidation of $\Delta_2\Lambda'/\Lambda_2\Delta'$-[{Ru(bpy)$_2$}$_2$Os(bpy)$_2$}($\mu$-HAT)]$^{n+}$ (n = 6−9) at −15 °C. (a) Spectroelectrochemical changes for the oxidation reaction $\Delta_2\Lambda'/\Lambda_2\Delta'$-[{Ru(bpy)$_2$}$_2$Os(bpy)$_2$}($\mu$-HAT)]$^{6+}$ → $\Delta_2\Lambda'/\Lambda_2\Delta'$-[{Ru(bpy)$_2$}$_2$Os(bpy)$_2$}($\mu$-HAT)]$^{7+}$. The inset shows NIR band (—) of the latter in addition to the bands obtained from Gaussian deconvolution (· · ·). (b) Spectroelectrochemical changes for the oxidation reaction $\Delta_2\Lambda'/\Lambda_2\Delta'$-[{Ru(bpy)$_2$}$_2$Os(bpy)$_2$}($\mu$-HAT)]$^{7+}$ → $\Delta_2\Lambda'/\Lambda_2\Delta'$-[{Ru(bpy)$_2$}$_2$Os(bpy)$_2$}($\mu$-HAT)]$^{8+}$. The inset shows the NIR spectrum (- · -) of the latter in addition to the bands obtained from Gaussian deconvolution (· · ·). (c) Summary of the spectra of $\Delta_2\Lambda'/\Lambda_2\Delta'$-[{Ru(bpy)$_2$}$_2$Os(bpy)$_2$}($\mu$-HAT)]$^{n+}$.

The spectra of the +6 states of the dinuclear complexes are characterized by intense π(bpy) → dπ(M^{III}) and π(HAT) → dπ(M^{III}) LMCT absorptions in the 10 000−16 000 cm^{-1} region. The homo-dinuclear diastereoisomers exhibit a single LMCT transition at ∼14 200 cm^{-1}, while the hetero-dinuclear diastereoisomers exhibit two LMCT transitions at ∼10 760 and 13 260 cm^{-1} which involve the Ru and Os centers, respectively. The latter is consistent with the LMCT transition at 10 400 cm^{-1} in [Os(bpy)$_2$(HAT)]$^{3+}$.

Spectroelectrochemical oxidation of the trinuclear complexes allowed the generation of the mixed-valence +7 and +8 forms and fully oxidized +9 forms at −15°C (Figure 4). Stable isosbestic points were observed in the spectral progressions accompanying the three stages of oxidation. The ^{1}MLCT absorption bands decreased in intensity following one- and two-electron oxidation, and disappeared completely on further oxidation to the +9 species. The dπ(Os^{II}) →

π^*(HAT) ^{3}MLCT transition at 12 235 cm^{-1} disappeared completely following oxidation of the Os^{II} center. The bands in the 10 000−16 000 cm^{-1} region which gained intensity upon oxidation were assigned as LMCT transitions by comparison with the spectra of the mono- and dinuclear analogues.

Intervalence Charge Transfer. The IVCT band parameters obtained from the Gaussian deconvolution of the NIR spectra for the partially oxidized mixed-valence and the fully oxidized systems are provided in Tables S8 and S9 (Supporting Information), respectively.

Dinuclear Systems. The NIR spectra of the homo-dinuclear and hetero-dinuclear osmium systems $[\{M(bpy)_2\}(\mu\text{-HAT})\{Os(bpy)_2\}]^{n+}$ (M = Ru or Os, n = 5, 6) exhibit an added complexity in behavior compared with the analogous homo-dinuclear ruthenium systems[20] because of the larger spin−orbit coupling constant for Os^{III} relative to that of Ru^{III} ($\xi_{Os} \approx 3000$ cm^{-1} vs $\xi_{Ru} \approx 1000$ cm^{-1}),[51] which is manifested by multiple absorption bands resulting from IVCT and IC (interconfigurational) transitions in the NIR region of the +5 and +6 spectra (Tables S8 and S9, Figure 3).

The one-electron oxidation of $[\{Os(bpy)_2\}_2(\mu\text{-HAT})]^{4+}$ resulted in the appearance of two new bands in the 3500−10 000 cm^{-1} region (ν_{max} = 4960 and 8195 cm^{-1} (meso), 4950 and 8200 cm^{-1} (rac)). The more intense, higher-energy band disappeared completely on removal of the second electron and was assigned as an IVCT transition (Table S9, Figure 4). This band appears asymmetrical and narrower on the lower-energy side; Gaussian deconvolution revealed the presence of two underlying transitions at 8200 and 8780 cm^{-1} (meso) and 9260 and 9130 cm^{-1} (rac), with the transition moment for the first component being a factor of 4 greater than the second.

Compared with the theoretical bandwidths ($\Delta\nu_{1/2}^\circ$ in eq 2) of 3880 cm^{-1} for the transitions at 8200 and 8260 cm^{-1} in *meso*- and *rac*-$[\{Os(bpy)_2\}_2(\mu\text{-HAT})]^{5+}$, respectively, the relatively narrow observed bandwidths are indicative of significant electronic communication between the metal centers. Indeed, the electrochemical and spectral features of diastereiosomers of $[\{Os(bpy)_2\}_2(\mu\text{-HAT})]^{n+}$ (n = 5, 6) are strikingly similar to those detailed previously for the Os analogue of the Creutz−Taube ion, $[\{Os(NH_3)_5\}_2(\mu\text{-pyz})]^{5+}$, which has been analyzed by assuming complete delocalization.[52−55] The greater dπ orbital extension for Os enhances the intrametal electronic coupling in $[\{Os(bpy)_2\}_2(\mu\text{-HAT})]^{5+}$ relative to the Ru analogue[20] and leads to a delocalized ground state in the former. The electronic coupling parameter, H_{ab}, is estimated as 4100 and 4130 cm^{-1} for the IVCT transitions in the meso (8200 cm^{-1} band) and rac (8260 cm^{-1} band) diastereoisomers, respectively, since $H_{ab} = 1/2\nu_{max}$ for delocalized complexes.[56] In this delocalized description, the explicit consideration of the third electronic state identified with the bridging ligand is essential, and the origin of the transition is more adequately described as a transition between bonding and antibonding orbitals within the molecular manifold of the system, as described by Ondrechen and depicted in Figure S5 (Supplementary Information).[57−63]

The appearance of d$\pi \rightarrow$ dπ transitions between the dπ-(Os^{III}) orbitals which are split by spin−orbit coupling have been used as a diagnostic marker for localized oxidation states.[52−55] The NIR spectra of $[\{Os(bpy)_2\}_2(\mu\text{-HAT})]^{6+}$ exhibit IC transitions in the 4000−5500 cm^{-1} region which are slightly red shifted and of greater intensity than those in the mononuclear analogue $[Os(bpy)_2(HAT)]^{3+}$ (Figure S4 and Table S9). In the dinuclear complex, electronic delocalization across the bridging ligand decreases the energy splittings between the dπ(Os^{III}) levels and enhances the intensities of the IC transitions by mixing the charge-transfer character of the adjacent Os(II) center into the nominally d$\pi \rightarrow$ dπ transitions.[7,34,51,64−68] The mixed-valence species lack the IC bands in their NIR spectra, thus supporting a delocalized classification. The relatively low-intensity, asymmetric band in the 5000−6600 cm^{-1}region is tentatively assigned as a vibronic component associated with intense absorptions that are expected to occur outside the limit of detection in the IR region.

Because of the enhanced spin−orbit coupling in the homo-dinuclear osmium complex relative to the $[\{Ru(bpy)_2\}_2(\mu\text{-HAT})]^{5+}$ systems,[20] larger energy separations between the three IVCT transitions are expected. In the homo-dinuclear Ru complex, the three underlying components in the IVCT band (IVCT(1)−(3) in order of increasing energy) were identified as spin−orbit transitions in a localized description. The separation between the components ($\Delta E_{so(1)}$ and $\Delta E_{so(2)}$) represent the $\Delta E'$ contribution to ν_{max} in eq 1.[7,51] The IC bands for the analogous Ru complex are not observed over the spectral range investigated as the lesser magnitude of ξ_{Ru} has the effect of shifting the IC transitions into the infrared region and decreasing their absorptivity.[7,34] In the localized limit, eq 3 expresses the semiquantitative energy relationships between the IVCT and IC bands,[7] where $\Delta E_{so(1)}$ and $\Delta E_{so(2)}$ are the energies of the IC bands and their

(51) Kober, E. M.; Goldsby, K. A.; Narayana, D. N. S.; Meyer, T. J. *J. Am. Chem. Soc.* **1983**, *105*, 4303−4309.
(52) Magnuson, R. H.; Lay, P. A.; Taube, H. *J. Am. Chem. Soc.* **1982**, *105*, 2507−2509.
(53) Magnuson, R. H.; Lay, P. A.; Taube, H. *J. Am. Chem. Soc.* **1983**, *105*, 2507−2509.
(54) Lay, P. A.; Magnuson, R. H.; Taube, H. *Inorg. Chem.* **1988**, *27*, 2364−2371.
(55) Dubicki, L.; Ferguson, J.; Krausz, E. R.; Lay, P. A.; Maeder, M.; Taube, H. *J. Phys. Chem.* **1984**, *88*, 3940−3941.
(56) Hush, N. S. *Coord. Chem. Rev.* **1985**, *64*, 135.
(57) Zhang, L.-T.; Ko, J.; Ondrechen, M. J. *J. Phys. Chem.* **1989**, *93*, 3030−3034.
(58) Root, L. J.; Ondrechen, M. J. *Chem. Phys. Lett.* **1982**, *93*, 421−424.
(59) Ko, J.; Ondrechen, M. J. *Chem. Phys. Lett.* **1984**, *112*, 507−512.
(60) Ondrechen, M. J.; Ko, J.; Root, L. J. *J. Phys. Chem.* **1984**, *88*, 5919−5923.
(61) Ko, J.; Ondrechen, M. J. *J. Am. Chem. Soc.* **1985**, *107*, 6161−6167.
(62) Ondrechen, M. J.; Ko, J.; Zhang, L.-T. *J. Am. Chem. Soc.* **1987**, *109*, 1672−1676.
(63) Zhang, L.-T.; Ko, J.; Ondrechen, M. J. *J. Am. Chem. Soc.* **1987**, *109*, 1666−1671.
(64) Kober, E. M.; Meyer, T. J. *Inorg. Chem.* **1982**, *21*, 3967−3977.
(65) Neyhart, G. A.; Timpson, C. J.; Bates, W. D.; Meyer, T. J. *J. Am. Chem. Soc.* **1996**, *118*, 3730−3737.
(66) Demadis, K. D.; Neyhart, G. A.; Kober, E. M.; Meyer, T. J. *J. Am. Chem. Soc.* **1998**, *120*, 7121−7122.
(67) Demadis, K. D.; El-Samanody, E.-S.; Coia, G. M.; Meyer, T. J. *J. Am. Chem. Soc.* **1999**, *121*, 535−544.
(68) Demadis, K. D.; Neyhart, G. A.; Kober, E. M.; White, P. S.; Meyer, T. J. *Inorg. Chem.* **1999**, *38*, 5948−5959.

separation is approximately equal to the energy difference between IVCT(2) and IVCT(3).

$$\Delta E_{so(1)} \approx \nu_{max}\{\text{IVCT(2)}\} - \nu_{max}\{\text{IVCT(1)}\}$$
$$\Delta E_{so(2)} \approx \nu_{max}\{\text{IVCT(3)}\} - \nu_{max}\{\text{IVCT(1)}\} \quad (3)$$

On the basis of the semiquantitative relationships expressed in eq 3, if the transitions at 8200 and 8780 cm^{-1} in *meso*-$[\{Os(bpy)_2\}_2(\mu\text{-HAT})]^{5+}$ are assigned as IVCT(2) and IVCT-(3), respectively, then IVCT(1) is expected to occur at ~3880 cm^{-1} {i.e., IVCT(2) − $\Delta E_{so(1)}$}. Indeed, the increased absorptivity in this range near the detector limit raises the possibility that IVCT(1) lies at the detector limit.

In the diastereoisomers of $[\{Ru(bpy)_2\}(\mu\text{-HAT})\{Os(bpy)_2\}]^{4+}$, one-electron oxidation results in the mixed-valence species which is characterized by a broad Gaussian-shaped IVCT band at 8610 and 8695 cm^{-1} in the pseudo-meso and rac diastereoisomers, respectively. Two bands are also evident at 4080 and 4880 cm^{-1} (pseudo-meso) and 4060 and 4880 cm^{-1} (rac), with the lower-energy band exhibiting an intensity enhancement of a factor of 3 compared with the higher energy component. The latter coincides with the position of the vibronic transitions in $[\{Os(bpy)_2\}_2(\mu\text{-HAT})]^{5+}$. The higher-energy transition provides evidence for a localized Os^{III} site in the hetero-dinuclear complex and the mixed-valence formulation $[\{Ru^{II}(bpy)_2\}(\mu\text{-HAT})\{Os^{III}(bpy)_2\}]^{5+}$. The IC bands experience a slight blue-shift following two-electron oxidation because of the destabilization and increased splitting of the $d\pi(Os^{III})$ orbitals.

The IVCT band in the hetero-dinuclear complex occurs at higher energy than the analogous homo-dinuclear systems because of the additional redox asymmetry (ΔE_0) contribution to ν_{max}. According to Meyer and Goldsby,[49] ΔE_0 may be estimated from the semiquantitative relationship in eq 4, assuming that the additional contributions to ΔE_{ox} (e.g., solvation energies) are similar for the closely structurally related systems.[49] The estimate of 2840 cm^{-1} (viz. 352 mV)

$$\Delta(\Delta E_{ox}) = \Delta E_{ox}(Ru^{II}/Os^{III}) - \Delta E_{ox}(Ru^{II}/Ru^{III}) \quad (4)$$

for both diastereoisomers is in poor agreement with the difference of 3330 cm^{-1} between the maxima of the IVCT manifolds in the $[\{Ru(bpy)_2\}_2(\mu\text{-HAT})]^{5+}$ and $[\{Ru(bpy)_2\}(\mu\text{-HAT})\{Os(bpy)_2\}]^{5+}$ systems. The discrepancy is likely to originate from the extensive electronic coupling in the systems, which invalidates the weak coupling approximation (implicit in eq 4), in addition to differences in the solvation and ion-pairing energies for the two complexes.[49,50]

On the basis of a classical analysis, the degree of electronic coupling (H_{ab}) in the diastereoisomers of $[\{Ru(bpy)_2\}(\mu\text{-HAT})\{Os(bpy)_2\}]^{5+}$ was determined from eq 5 where r_{ab} is the diabatic metal−metal distance (i.e., the intermetal distance in the hypothetical absence of electronic coupling). In the present case, r_{ab} was assumed to be equal to the geometrical metal−metal distance obtained from the X-ray crystal structure of the cation[56] such that the H_{ab} values obtained from eq 5 are estimates only of the actual electronic coupling.

$$H_{ab} = \frac{2.06 \times 10^{-2}(\nu_{max}\epsilon_{max}\Delta\nu_{1/2})^{1/2}}{r_{ab}} \quad (5)$$

The H_{ab} values of 400 and 360 cm^{-1} for the pseudo-meso and rac diastereoisomers, respectively, reveal that the degree of electronic delocalization in the hetero-dinuclear species is substantially reduced compared with that in the analogous homo-dinuclear Ru and Os systems. Electronic coupling is dominated by mixing between the Ru orbitals and the π^*-(HAT) orbitals in the hetero-dinuclear system, and the relatively lower energy of the $d\pi$(Ru) orbital compared with $d\pi$(Os) gives rise to decreased coupling through the bridging ligand.[46]

Trinuclear Systems. The two mixed-valence states of $\Delta_2\Lambda'/\Lambda_2\Delta'$-$[\{Ru(bpy)_2\}_2\{Os(bpy)_2\}(\mu\text{-HAT})]^{n+}$ ($n = 7, 8$) were generated upon one- and two-electron oxidation of the +6 species at −15 °C. The mixed-valence species $[\{Ru^{II}(bpy)_2\}_2\{Os^{III}(bpy)_2\}(\mu\text{-HAT})]^{7+}$ is characterized by a broad Gaussian-shaped IVCT band at 7670 cm^{-1} that is slightly overlapping with a weak transition at 9480 cm^{-1}. Gaussian deconvolution reveals the presence of two IC $d\pi \rightarrow d\pi$ bands at 3975 and 4620 cm^{-1} which were assigned by analogy with the spectra of the $[\{Ru(bpy)_2\}(\mu\text{-HAT})\{Os(bpy)_2\}]^{5+}$ diastereoisomers. The appearance of these bands provides evidence for a localized Os^{III} site.

The IVCT band in $\Delta_2\Lambda'/\Lambda_2\Delta'$-$[\{Ru(bpy)_2\}_2\{Os(bpy)_2\}(\mu\text{-HAT})]^{7+}$ is expected to occur at higher energy than the $[\{Ru(bpy)_2\}_3(\mu\text{-HAT})]^{7+}$ systems. A semiquantitative analysis yields an estimate of 2550 cm^{-1} for the ΔE_0 contribution in the hetero-trinuclear system (viz. from eq 4, $\Delta(\Delta E_{ox}) = \Delta E_{ox(2-1)}(Ru_2Os) - \Delta E_{ox(3-2)}(\text{heterochiral } Ru_3)$).[49] On this basis, an IVCT transition in the homo-trinuclear systems is predicted at ~5120 cm^{-1}, which corresponds to the observed average energy of the two major components (IVCT(1) and (2)) of the IVCT manifold. Given the localized nature of the IVCT transitions in the hetero-trinuclear complex, the previously well-resolved IVCT(1) and (2) components in the homo-trinuclear diastereoisomers[20] are overlapped to a greater extent in the former case and are observed as a single Gaussian band. If the transition at 9480 cm^{-1} is assigned as an IVCT component in the hetero-trinuclear system, then a corresponding band at 6930 cm^{-1} is predicted in the homochiral system, which lies close to the observed IVCT-(3) at 7160 cm^{-1}. The component at 9480 cm^{-1} exhibits a relatively low intensity, as the origin of the transition is a $d\pi_3-\pi^*(HAT)-d\pi_3$ interaction between orbitals which are largely d_{xy} in character.

On the basis of a classical analysis, $\Delta\nu_{1/2}°$ and H_{ab} for the IVCT band at 7670 cm^{-1} in $[\{Ru(bpy)_2\}_2\{Os(bpy)_2\}(\mu\text{-HAT})]^{7+}$ are determined to be 3190 and 450 cm^{-1}, respectively (where r_{ab} is equated with the geometrical metal−metal distance from the X-ray crystal structure of the hetero-dinuclear diastereoisomer). The results suggest that the degree of electronic delocalization is slightly less than that for the diastereoisomers of $[\{Ru(bpy)_2\}_3(\mu\text{-HAT})]^{7+}$ and is similar to that in the diastereoisomers of $[\{Ru(bpy)_2\}(\mu\text{-HAT})\{Os(bpy)_2\}]^{5+}$.

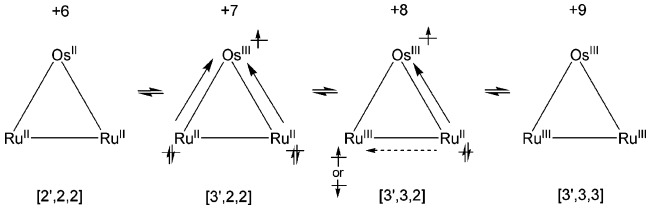

Figure 5. Schematic illustration of the proposed origins of the IVCT transitions in the +7 and +8 mixed-valence forms of $[\{Ru(bpy)_2\}_2\{Os(bpy)_2\}(\mu\text{-HAT})]^{n+}$ ($n = 6-9$). The formal oxidation states of the metal centers are shown in square brackets where the primes denote the Os center and the solid and dashed arrows illustrate the Os−Ru and Ru−Ru interactions, respectively. The occupancy of the highest-occupied molecular orbitals of the formally Ru^{2+} (doubly occupied, spin-paired) and M^{3+} (M = Ru or Os, singly occupied, spin-unpaired) centers is also indicated.

Deconvolution of the NIR spectrum of $[\{Ru(bpy)_2\}_2\{Os(bpy)_2\}(\mu\text{-HAT})]^{8+}$ reveals the presence of IVCT transitions at 5530 and 7765 cm^{-1} between Ru^{II} and the Ru^{III} and Os^{III} centers, respectively (Figure 4, Table S9). The transition between adjacent Ru^{II} and Os^{III} centers is slightly blue shifted compared with the transition of the same origin in $[\{Ru(bpy)_2\}(\mu\text{-HAT})\{Os(bpy)_2\}]^{5+}$. The +8 mixed-valence state in the hetero-trinuclear complex is also characterized by two new bands at 10 550 and 13 110 cm^{-1}. The latter is assigned as an LMCT transition and occurs at a similar energy to the bands of the same origin in the hetero-dinuclear analogue. The band at 10 550 cm^{-1} is tentatively assigned as an IVCT transition and decreases upon subsequent oxidation to the +9 state. As described previously for the homo-trinuclear analogue, the IVCT transitions may correspond to the formation of either singlet or triplet "exciton" states; however, definitive assignments are not possible in the present case because of the highly convoluted nature of the spectra. While the assignments for the NIR region in the +8 species are ambiguous because of the presence of complicating comproportionation equilibria, the bands in the energy region below 5500 cm^{-1} may be reasonably ascribed to IC transitions at Os^{III}. In general, the presence of the third metal center in the hetero-trinuclear system has the effect of decreasing the effective charge density available for the IVCT processes, resulting in IVCT and IC transitions that are less intense than those observed in the dinuclear $[\{Ru(bpy)_2\}(\mu\text{-HAT})\{Os(bpy)_2\}]^{5+}$ analogue.

Conclusions

The IVCT properties of the dinuclear species, $[\{Os(bpy)_2\}_2(\mu\text{-HAT})]^{5+}$ and $[\{Ru(bpy)_2\}(\mu\text{-HAT})\{Os(bpy)_2\}]^{5+}$, and the trinuclear species, $\Delta_2\Lambda'/\Lambda_2\Delta'\text{-}[\{Ru(bpy)_2\}_2\{Os(bpy)_2\}(\mu\text{-HAT})]^{6+}$, display a marked dependence on the nuclearity and extent of oxidation of the mixed-valence assemblies. Small differences are also observed between the diastereoisomers of the same complex in the dinuclear cases.

The IVCT properties of $[\{Ru(bpy)_2\}_2\{Os(bpy)_2\}(\mu\text{-HAT})]^{n+}$ ($n = 7, 8$) are intermediate between those of the localized mixed-valence complex $[\{Ru(bpy)_2\}(\mu\text{-HAT})\{Os(bpy)_2\}]^{5+}$ and the analogous oxidation-state isomer of $[\{Ru(bpy)_2\}_3(\mu\text{-HAT})]^{n+}$ ($n = 7, 8$).[20] The NIR spectrum of the +7 state of the hetero-trinuclear mixed-valence species exhibits both IC and IVCT transitions which are quantitatively similar to those in $[\{Ru(bpy)_2\}(\mu\text{-HAT})\{Os(bpy)_2\}]^{5+}$ and are indicative of the localized mixed-valence formulation $[\{Ru^{II}(bpy)_2\}_2\{Os^{III}(bpy)_2\}(\mu\text{-HAT})]^{7+}$. The +8 state exhibits IVCT and IC transitions which are indicative of both localized and delocalized behavior. The origins of the IVCT transitions in the mixed-valence states of $[\{Ru(bpy)_2\}_2\{Os(bpy)_2\}(\mu\text{-HAT})]^{n+}$ are depicted in Figure 5. The localized nature of the IVCT transitions in the hetero-trinuclear species is in contrast to the situation in the diastereoisomers of $[\{Ru(bpy)_2\}_3(\mu\text{-HAT})]^{n+}$ which exhibit extensive electronic communication between the metal centers.[20]

Qualitatively, a localized description based on the geometrical properties of the $d\pi(Os^{II/III})$ and $d\pi(Ru^{II/III})$ orbitals which accounts for the redox asymmetry contribution provides a reasonable rationale for the IC and IVCT behavior in the hetero-dinuclear and hetero-trinuclear mixed-valence systems. However, the diastereoiosmers of $[\{Os(bpy)_2\}_2(\mu\text{-HAT})]^{5+}$ exhibit extensive electronic delocalization, and the description of their mixed-valence properties requires a delocalized description which explicitly includes vibronic coupling.

The detailed analysis of IVCT in trinuclear complexes provides a foundation for the theoretical treatment and elucidation of multisite interactions in extended arrays and metallosupramolecular systems which have been proposed as the basis of novel molecular materials.[69−71]

Acknowledgment. This work was supported by the Australian Research Council.

Supporting Information Available: Tables of crystal data and structure refinement parameters for $\Lambda\Delta/\Delta\Lambda\text{-}[\{Ru(bpy)_2\}(HAT)\{Os(bpy)_2\}](PF_6)_3Cl$, atomic coordinates, hydrogen atom coordinates, anisotropic thermal parameters, bond lengths and bond angles; redox potentials for the reductions based on the HAT bridging ligand for the di- and trinuclear complexes; deconvoluted NIR spectral data of the reduced absorption spectra (ϵ/ν vs ν) for the di- and trinuclear complexes; and deconvoluted NIR spectral data (ϵ/ν vs ν) of the fully oxidized forms of the mono- and dinuclear complexes. Figures showing proton numbering schemes for ΛΔ- and ΔΔ-$[\{M(bpy)_2\}(\mu\text{-HAT})\{M'(bpy)_2\}]^{4+}$ {M,M′ = Os,Os or Ru,-Os}; structure of the ΛΔ-$[\{M(bpy)_2\}(\mu\text{-HAT})\{M'(bpy)_2\}]^{4+}$ cation showing the association of two PF_6^- anions within the clefts between the bpy ligands; schematic illustration of the relative potentials of the metal-based oxidation processes in selected mono-, di-, and trinuclear ruthenium and osmium complexes in this study; UV−vis/NIR spectra of $[Os(bpy)_2(HAT)]^{n+}$ ($n = 2,2$) at −35 °C; and qualitative molecular orbital diagram for the dinuclear $[\{Ru(bpy)_2\}_2(\mu\text{-BL})]^{5+}$ systems. This material is available free of charge via the Internet at http://pubs.acs.org.

IC051699I

(69) Balzani, V.; Juris, A.; Venturi, M.; Campagna, S.; Serroni, S. *Chem. Rev.* **1996**, *96*, 759−833.
(70) Belser, P.; Bernhard, S.; Blum, C.; Beyeler, A.; De Cola, L.; Balzani, V. *Coord. Chem. Rev.* **1999**, *190*, 0−192, 155−169.
(71) Garcia, C. G.; de Lima, J. F.; Iha, N. Y. M. *Coord. Chem. Rev.* **2000**, *196*, 219−247.